Noise-Tolerant Instantaneous Heart Rate and R-peak Detection Using Short-term Autocorrelation for Wearable Healthcare Systems*

Takahide Fujii, Masanao Nakano, *Student Member, IEEE*, Ken Yamashita, Toshihiro Konishi,
Student Member, IEEE, Shintaro Izumi, Hiroshi Kawaguchi, and Masahiko Yoshimoto, *Members, IEEE*

Abstract—This paper describes a robust method of Instantaneous Heart Rate (IHR) and R-peak detection from noisy electrocardiogram (ECG) signals. Generally, the IHR is calculated from the R-wave interval. Then, the R-waves are extracted from the ECG using a threshold. However, in wearable bio-signal monitoring systems, noise increases the incidence of misdetection and false detection of R-peaks. To prevent incorrect detection, we introduce a short-term autocorrelation (STAC) technique and a small-window autocorrelation (SWAC) technique, which leverages the similarity of QRS complex waveforms. Simulation results show that the proposed method improves the noise tolerance of R-peak detection.

I. INTRODUCTION

Mobile health is expected to play an increasingly prominent role in health provision because of the advent of an aging society [1]. Especially, daily life monitoring is important to prevent lifestyle diseases, which raise the number of patients and elderly people who need nursing care. This report specifically describes noise-tolerant IHR and the R-peak detection algorithm for a wearable ECG monitoring system. The IHR, an important bio-signal, is useful for heart disease detection, heart rate variation analysis [2], and exercise intensity estimation [3].

The key factors affecting wearable system usability are miniaturization and weight reduction. However, strict limitations on power consumption and electrode distance of wearable ECG monitors renders them sensitive to various noises. Especially, the signal-to-noise ratio (SNR) of ECG signals of moving (e.g. exercising) subjects is degraded.

Sophisticated analog front-end circuits are generally necessary to prevent SNR degradation. The analog front-end of the ECG monitoring system mainly comprises amplifiers, analog filters, and an analog-to-digital converter (ADC). Unfortunately, analog circuits are large, with high power consumption. Battery mass and power consumption must be reduced because battery mass dominates wearable systems.

Amplifiers have a tradeoff between power consumption and performance (e.g., gain, phase characteristic, common mode rejection ratio). Moreover, the analog filter in an ECG monitor has a large RC time constant because the frequency range of ECG signals is low (less than 1 kHz). Consequently,

it is difficult to use a high-performance amplifier and analog filters, which have a high quality factor.

Ultra-low-power ADCs, which have sub-μW power consumption and limited sample rate, have been developed for biomedical applications [4, 5]. Furthermore, according to Moore's law, the power of digital components increases with the progress of process technology. However, the power consumption of analog circuits will not decrease similarly. Therefore, the feature and purpose of our approach is the use of digital signal processing to reduce the performance requirements of analog components and to minimize the entire system's power consumption.

II. CONVENTIONAL IHR AND R-PEAK DETECTION

Extracting R-waves with a threshold determination is a general approach. Recently, various statistical approaches have been proposed for noise-tolerant threshold calculation such as using root-mean-squares (RMS) [6], standard deviations (SD), and mean deviations (MD) [7].

Some preprocessing techniques for noise reduction from an ECG signal have been proposed such as a band pass filter, an adaptive filter [8], a Kalman filter [9], a discrete wavelet transform (DWT) [6, 10], and neural networks [11]. They are used in advance of threshold calculation to mitigate noise intensity and to improve the R-wave detection success rate.

Autocorrelation [12, 13] and template matching [14] are more robust approaches because these algorithms utilize the similarity of QRS complex waveforms and have no threshold calculation process. Previously, autocorrelation was used in a non-invasive monitoring system [15]. However, the method requires numerous computations because it calculates the average heart-rate over a long duration (30 s).

In our previous work, a short-term autocorrelation (STAC) technique has been proposed for IHR detection [16]. This algorithm is applied after preprocessing, which utilizes the quadratic spline wavelet transform (QSWT) [10]. The QSWT requires few calculations and little hardware cost because it can be implemented using only adders and shift operators. Fig. 1 presents frequency characteristics of the QSWT with 128-Hz sampling rate. The base-line wander and hum noise can be removed easily using QSWT. Unfortunately, the frequency range of the muscle artifact and electrode motion artifact resemble the desired ECG signals. Therefore, the STAC is applied to extract the IHR from output signal of QSWT (Q_w). As shown in Fig. 2 and (1–4), the IHR at time t_n (IHR_n) is obtained as a window shift length (T_{shift}) that maximizes the correlation coefficient between the template window and the search window (CC^n_{ST}).

T. Fujii, M. Nakano, K. Yamashita, T. Konishi, S. Izumi, H. Kawaguchi, and M. Yoshimoto are with Kobe University, 1-1-Rokkodai Nada Kobe Hyogo Japan (corresponding author to provide phone/fax: 078-803-6629; e-mail: fujii@cs28.cs.kobe-u.ac.jp).
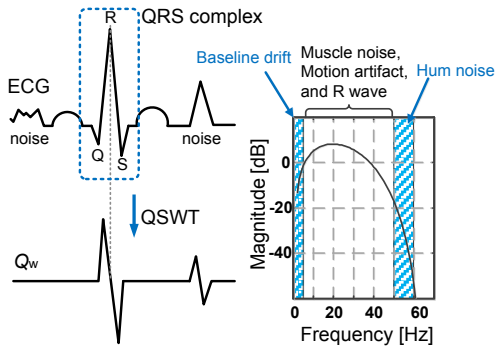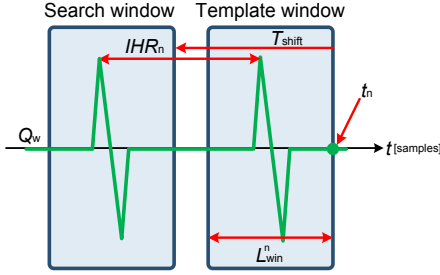
Figure 1.   Frequency charactaristics of QSWT.

Figure 2.   IHR detection using STAC.

$$CC_{ST}^{n}\left[T_{shift}\right]=w_1\cdot\sum_{i=0}^{L_{win}^{n}-1}Q_w[t_n-i]\cdot Q_w[(t_n-T_{shift})-i] \qquad (1)$$

$$IHR_n=\arg_{T_{shift}}\max_{0.25\times F_s\le T_{shift}\le 1.5\times F_s}\left\{CC_{ST}^{n}\left[T_{shift}\right]\right\} \qquad (2)$$

$$L_{win}[n+1]=\begin{cases}IHR[n]\cdot(1.2)^3 & (IHR[n]<0.316\times F_s)\\ IHR[n]\cdot(1.2)^2 & (0.316\times F_s\le IHR[n]<0.695\times F_s)\\ IHR[n]\cdot(1.2) & (0.695\times F_s\le IHR[n])\end{cases} \qquad (3)$$

$$w_1=\begin{cases}1 & (T_{shift}\le 0.546\times F_s)\\ 0.75 & (0.546\times F_s<T_{shift}\le 0.983\times F_s)\\ 0.5 & (0.983\times F_s<T_{shift})\end{cases} \qquad (4)$$

In the equations above, F_s, L_{win}, and w_1 respectively denote the sampling rate (samples/s), the window length, and the weight coefficient. The value of T_{shift} is set as 0.25 s to 1.5 s because the heart rate of a healthy subject is from 40 bpm to 240 bpm. The L_{win} is updated according to the estimated IHR to reduce the computational amount and to improve the accuracy of IHR estimation. Then, the range of L_{win} and w_1 is determined by the maximum rate of beat-to-beat variation, which is generally 20% in a healthy subject [16].

III. PROPOSED METHOD

The conventional STAC is optimized for IHR detection. Identifying the exact position of QRS complex in the template window is difficult. This report describes an extended algorithm of STAC that can extract not only the IHR but also R-peaks. Fig. 3 shows a block diagram of the proposed method.

A. IHR Detection with STAC

First, IHR is calculated using QSWT and STAC.

$$CC_{ST}^{n}\left[T_{shift}\right]=w_1\cdot\sum_{i=0}^{L_{win}^{n}-1}w_2\cdot Q_w[t_n-i]\cdot Q_w[(t_n-T_{shift})-i] \qquad (5)$$

$$IHR_n=\arg_{T_{shift}}\max_{T_{min}^{n}\le T_{shift}\le T_{max}^{n}}\left\{CC_{ST}^{n}\left[T_{shift}\right]\right\} \qquad (6)$$

$$T_{max}^{n}=\begin{cases}1.25\times IHR_{n-1} & (IHR_{n-1}\le 1.2\times F_s)\\ 1.5\times F_s & (IHR_{n-1}>1.2\times F_s)\end{cases} \qquad (7)$$

$$T_{min}^{n}=\begin{cases}0.75\times IHR_{n-1} & (IHR_{n-1}\ge\frac{1}{3}F_s)\\ 0.25\times F_s & (IHR_{n-1}<\frac{1}{3}F_s)\end{cases} \qquad (8)$$

$$w_2=\begin{cases}1 & (i<\frac{1}{4}L_{win}^{n})\\ 0.75 & (\frac{1}{4}L_{win}^{n}\le i<\frac{3}{4}L_{win}^{n})\\ 0.5 & (\frac{3}{4}L_{win}^{n}\le i)\end{cases} \qquad (9)$$

Compared with (1–4), parameters of T_{shift} range (T_{mix}^{n}, T_{max}^{n}) and weight coefficient w_2 are newly introduced in (5–9). Then, T_{mix}^{n} and T_{max}^{n} are updated according to the previous IHR. When multiple R-peaks are contained in the template window or search window, the recent R-peak is selected by weight coefficient w_2.

B. R-peak Detection with Small-Window Autocorrelation

In the next step, we introduce a small-window autocorrelation (SWAC) method for R-peak detection. When the search window is fixed at $T_{shift}=IHR_n$, both the template window and the search window contain the QRS complex at the same distance from the right edge of the window (see Fig. 4). Therefore, as shown in Fig. 5, the recent R-peak can be identified using the autocorrelation of small windows in the template and search window. The correlation coefficient of small windows at t_n (CC_{SW}^{n}) and T_{peak}^{n}, which maximize the value of CC_{SW}^{n}, are calculated as shown below.

$$CC_{sw}^{n}\left[T_{shift}^{'}\right]=\sum_{i=-\frac{L_{win}^{'}}{2}}^{\frac{L_{win}^{'}}{2}-1}Q_w[(t_n-T_{shift}^{'})-i]\cdot Q_w[(t_n-T_{shift}^{'}-IHR_n)-i] \qquad (10)$$

$$T_{peak}^{n}=\arg_{T_{shift}^{'}}\max_{\frac{L_{win}^{'}}{2}\le T_{shift}^{'}\le L_{win}^{n}-\frac{L_{win}^{'}}{2}+1}\left\{CC_{SW}^{n}\left[T_{shift}^{'}\right]\right\} \qquad (11)$$

The length of small window ($L_{win}^{'}$) should be set much smaller than that of L_{win}, and larger than the length of the QRS complex. For this study, $L_{win}^{'}$ was set to 0.1 s.
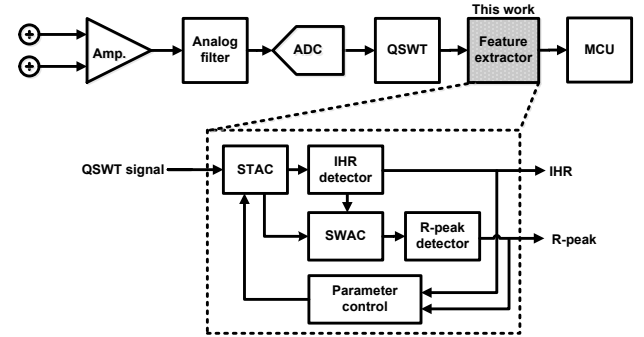

Figure 3.   Block diagram of proposed scheme.
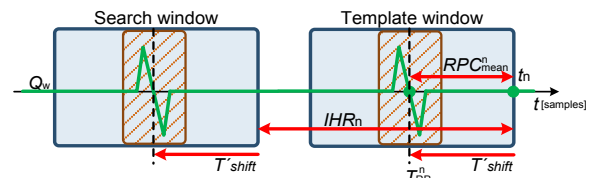

Figure 4.   Definition of small window.
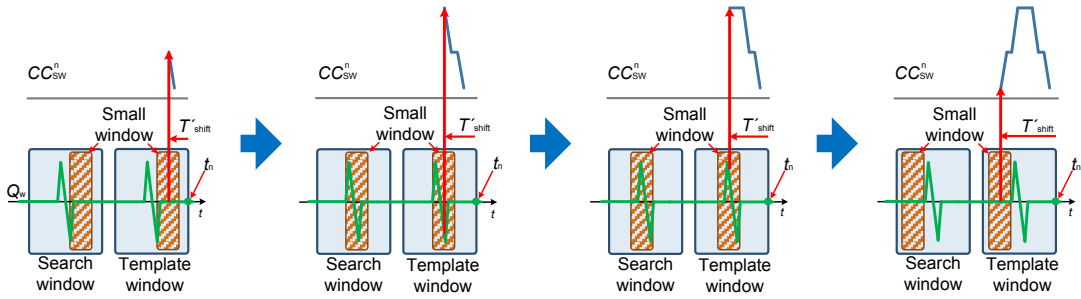
Figure 5.   QRS complex search using small-window autocorrelation (SWAC).

Although T^n_{peak} denotes the QRS complex, it does not mean the correct time of R-peak (T^n_{RP}) because L'_{win} is larger than the QRS complex. The value of CC^n_{SW} is almost the same while the small window contains QRS complex (see Fig. 5). To calculate the value of T^n_{RP} accurately, the set of R-peak candidates (RPC_n) is defined as described below.

$$RPC_n = \left\{ t \,\middle|\, CC^n_{SW}[t] \geq \frac{3}{4} CC^n_{SW}[T^n_{peak}], \, T^n_{peak} - \frac{L'_{win}}{2} \leq t \leq T^n_{peak} + \frac{L'_{win}}{2} \right\} \quad (12)$$

$$T^n_{RP} = t_n - RPC^n_{mean} \quad (13)$$

Here, the RPC^n_{mean} denotes the mean value of RPC_n. Fig. 6 presents the example of the T^n_{RP} calculation process.
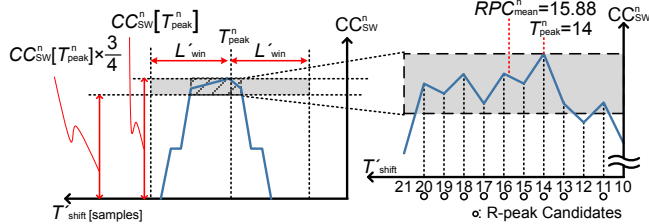

Figure 6.   R-peak detection using SWAC.

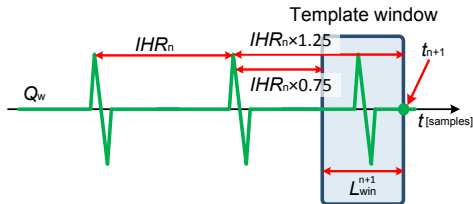Figure 7.   Parameter update of window length and evaluation time.

C. STAC Parameter Updating and Error Detection

Finally, next evaluation time (t_{n+1}) and L^{n+1}_{win} are updated using T^n_{RP}, as shown in Fig. 7 and (14, 15).

$$L^{n+1}_{win} = T^n_{max} - T^n_{min} \quad (14)$$

$$t_{n+1} = \begin{cases} t_n + F_s & \left(\begin{array}{l}\text{Initialization mode} \\ \text{and error recovery mode}\end{array}\right) \\ T^n_{RP} + T^n_{max} & \text{(otherwise)} \end{cases} \quad (15)$$

The objective of this update is minimization of the window length to reduce the computational amount.

If the template window does not include any R-peak caused by several errors related to noise or arrhythmia, then T^{n+1}_{min}, T^{n+1}_{max}, and L^{n+1}_{win} are respectively initialized to $0.25F_s$, $1.5F_s$, and $1.5F_s$. This error can be detected by the correlation coefficient between the template window and search window (CC^n_{ST}). The criterion of the error is that the

$2 \times CC^n_{ST}[IHR_n]$ must be smaller than the median of $CC^{n-i}_{ST}[IHR_{n-i}]$, ($1 \leq i \leq 5$). Then, t_{n+1} is also set to $t_n + F_s$.

IV.   PERFORMANCE EVALUATION

To verify the effects of the proposed method, we performed simulation experiments using the public ECG database (MIT-BIH arrhythmia database [17]) and the noise database (MIT-BIH noise stress test database [18]). Then, we modeled our proposed method and conventional threshold-based R-peak detection method [6], which is used in single-chip ECG monitoring system LSI [19], in MATLAB.

Fig. 8 shows the relation between intensity of muscle artifact noise and accuracy of R-peak detection. The signal-to-noise ratio (SNR) is defined as shown below.

$$SNR = 10\log\frac{S}{N \times a^2} \quad (16)$$

Here, S, N, and a are respectively defined as the signal power, frequency-weighted noise power, and scale factor [18].

The definition of the sensitivity (Se) is $Se = TP / (TP + FN)$. The definition of the positive predictivity ($+P$) is $+P = TP / (TP + FP)$ [6]. Then, TP, FN, and FP respectively denote the number of correct R-peak detection, the number of failures to detect the true R-peak, and the number of false detection.

As shown in Fig. 8, although the conventional method has higher sensitivity, the number of false detections increases rapidly with noise intensity. In contrast, the proposed method has higher positive predictivity of R-peak detection despite its use in noisy conditions. At 13 dB SNR, the positive predictivity is improved 19% with 1% sensitivity degradation. There is a similar trend in other waveforms. Fig. 9 portrays an example waveform of R-peak detection at 13 dB SNR with motion artifact noise.
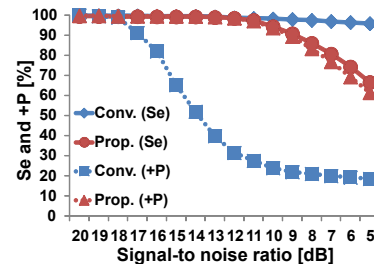

Figure 8.   Relation between SNR (MIT-BIH #123 with muscle artifact noise) and accuracy of R-peak detection. Conv.: threshold based R-peak detection [6]. Prop.: SWAC R-peak detection.
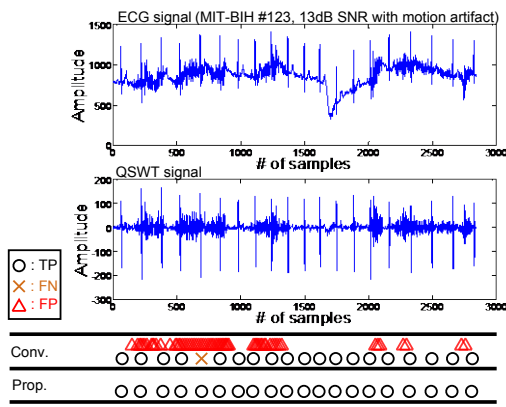
Figure 9. Example waveform of R-peak detection.

Table 1 presents a performance comparison of R-peak detection with various waveforms in various conditions. The proposed method improved 27.8% positive predictivity (from 67.9% to 95.7%) with 4.3% sensitivity degradation (from 96.5% to 92.3%) on average at 13 dB SNR with muscle artifact.

V. Conclusion

This paper explains a noise-tolerant IHR and R-peak detection algorithm using short-term autocorrelation. Simulation results show that the proposed algorithm improves noise tolerance compared with the conventional threshold method. Therefore, the proposed algorithm for digital processing can contribute to reduction of the minimum capacity and area of wearable ECG monitoring systems.

References

[1] H. Nakajima, T. Shiga, "Systems Health Care," In *Proc. of IEEE SMC*, pp. 1167-1172, Oct. 2011.

[2] W. Roel, M. John, "Comparing Spectra of a Series of Point Events Particularly for Heart Rate Variability Data," *IEEE Trans. Biomed. Eng.*, BME-31, no. 4, pp. 384-387, Apr. 1984.

[3] S. Yazaki, T. Matsunaga, "Evaluation of activity level of daily life based on heart rate and acceleration," In *Proc. of SICE*, pp. 1002-1005, Aug. 2010.

[4] M. van Elzakker, E. van Tuijl, P. Geraedts, et al., "A 1.9 uW 4.4 fJ/Conversion-Step 10 b 1 MS/s Charge - Redistribution ADC," *IEEE J-SSC*, vol. 45, no. 5, pp. 1007-1015, May 2010.

[5] P. Harpe, Y. Zhang, G. Dolmans, et al., "A 7-to-10b 0-to-4 ms/s Flexible SAR ADC With 6.5-to-16fJ/conversion-step," *IEEE ISSCC Dig. Tech. Papers*, pp. 472-473, Feb. 2012.

[6] H. Kim, R.F. Yazicioglu, et al., "ECG Signal Compression and Classification Algorithm with Quad Level Vector for ECG Holter System," *IEEE T-ITB.*, vol. 14, no. 1, pp. 93-100, Jan, 2010.

[7] J. P. Martinez, R. Almeida, S. Olmos, et al., "A wavelet-based ECG delineator: evaluation on standard databases," *IEEE Trans. Biomed. Eng.*, vol. 51, no. 4, pp. 570-581, Apr. 2004.

[8] P. S. Hamilton, W. J. Tompkins, "Adaptive matched filtering for QRS detection," In *Proc. of IEEE EMBC*, vol. 1, pp. 147-148, Nov. 1988.

[9] R. Vullings, B. De Vries, et al., "An Adaptive Kalman Filter for ECG Signal Enhancement, " *IEEE Trans. Biomed. Eng.*, vol58, no. 4, pp1094-1103, Apr. 2010.

[10] C. I. Ieong, M. I. Vai, P. U. Mak, P. I. Mak, "ECG Heart Beat Detection via Mathematical Morphology and Quadratic Spline Wavelet Transform," In *Proc. of IEEE ICCE*, pp. 609-610, Jan. 2011.

[11] Q. Xue, Y. H. Hu, W. J. Tompkins, "Neural-network-based adaptive matched filtering for QRS detection," *IEEE Tran. Biomed. Eng.*, vol. 39, no. 4, pp. 317-329, Apr. 1992.

[12] Y. Takeuchi, M. Hogaki, "An adaptive correlation rate meter: a new method for Doppler fetal heart rate measurements," *Ultrasonics*, pp. 127-137, May 1978.

[13] M. Sekine, K. Maeno, "Non-Contact Heart Rate Detection Using Periodic Variation in Doppler Frequency," In *Proc. of IEEE SAS*, pp. 318-322, Feb. 2011.

[14] H. L. Chan, G. U. Chen, M. A. Lin, and S. C. Fang, "Heartbeat Detection Using Energy Thresholding and Template Match," In *Proc. of IEEE EMBC*, pp. 6668-6670, Aug. 2005.

[15] M. Nakano, T. Konishi, et al., "Instantaneous Heart Rate detection using short-time autocorrelation for wearable healthcare systems, " In *Proc. of EMBC*, pp. 6703-6706, Aug. 2012.

[16] M. Malik, "Heart Rate Variability; standards of Measurement, Physiological Interpretation, and Clinical Use," *Circulation*, 1996; 93: 1043-1065.

[17] MIT-BIH Arrhythmia Database (mitdb), Record 100, "http://www.physionet.org/physiobank/database/mitdb/"

[18] MIT-BIH Noise Stress Test Database (nstdb), "http://www.physionet.org/physiobank/database/nstdb/"

[19] H. Kim, R. F. Yazicioglu, S. Kim, et al., "A configurable and low-power mixed signal SoC for portable ECG monitoring applications," *VLSI Symp.*, pp. 142-143, Jun. 2011.

TABLE I.   PERFORMANCE COMPARISON BETWEEN THRESHOLD BASED R-PEAK DETECTION [6] (CONV.) AND SWAC R-PEAK DETECTION (PROP.).

Tape (#)	w/o noise				muscle artifact SNR=13dB				motion artifact SNR=13dB			
	Sensitivity (%)		Positive predictivity (%)		Sensitivity (%)		Positive predictivity (%)		Sensitivity (%)		Positive predictivity (%)	
	Conv.	Prop.	Conv.	Prop.	Conv.	Prop.	Conv.	Prop.	Conv.	Prop.	Conv.	Prop.
100	100.0	98.6	100.0	99.9	99.9	98.7	95.3	99.8	99.4	98.5	85.1	99.8
101	99.9	99.5	99.5	99.8	99.8	99.1	90.8	99.6	99.2	99.1	69.8	99.6
102	98.4	96.7	60.5	97.3	97.6	93.4	49.9	94.8	95.7	95.4	32.0	96.0
103	99.7	99.9	100.0	100.0	99.7	99.9	92.1	100.0	99.1	99.8	77.4	100.0
104	97.8	89.8	58.7	95.2	96.8	72.3	40.9	80.7	95.8	81.3	26.4	87.0
105	98.8	95.3	88.2	98.6	98.8	93.5	71.5	97.5	98.9	95.3	48.0	98.4
106	92.6	75.8	97.3	97.5	93.7	74.2	76.0	91.3	94.1	73.8	49.1	92.2
107	97.7	94.9	50.7	99.6	97.0	90.2	34.7	95.1	97.9	92.6	23.6	97.2
108	70.8	79.4	34.1	82.4	71.6	76.6	25.3	79.3	73.9	77.0	17.0	79.9
109	99.5	97.3	70.4	99.4	99.4	96.6	57.0	99.2	99.5	97.0	39.4	99.3
111	88.2	98.0	55.9	98.4	88.1	97.5	38.2	98.3	88.5	97.0	25.1	98.2
112	100.0	99.6	99.9	100.0	100.0	99.5	83.3	100.0	99.0	99.5	52.4	100.0
113	100.0	98.2	100.0	98.8	100.0	97.6	92.7	98.2	99.3	97.7	70.6	98.4
114	98.6	96.6	98.1	98.9	98.9	95.2	70.6	97.3	97.9	96.0	35.8	98.0
115	99.9	99.0	100.0	99.5	100.0	98.8	90.6	99.4	99.1	98.2	62.1	99.1
116	98.8	93.7	99.2	99.5	98.3	89.9	78.6	97.1	98.3	90.8	48.9	97.8
117	97.8	99.0	98.9	99.0	97.5	97.3	60.6	97.3	95.2	98.0	25.5	98.5
118	99.5	94.8	55.2	99.7	99.1	93.5	40.2	98.7	99.6	94.7	27.5	99.5
119	99.3	67.3	83.9	93.1	98.8	64.5	74.1	80.4	98.7	66.5	50.8	85.2
121	96.9	99.4	95.0	99.9	96.9	98.1	61.7	99.1	99.4	99.2	32.3	99.9
122	90.8	100.0	100.0	100.0	92.2	99.9	88.0	99.9	96.2	100.0	62.3	100.0
123	99.8	99.5	100.0	99.8	99.9	98.6	79.7	98.9	99.2	98.9	39.8	99.2
124	96.5	97.7	97.3	99.4	96.2	97.5	69.8	98.9	97.7	97.0	33.4	99.1
Average	96.6	94.3	84.5	98.1	96.5	92.3	67.9	95.7	96.6	93.2	45.0	96.6
S.D.	6.3	8.4	20.6	3.7	6.0	9.9	20.7	6.3	5.4	9.1	18.6	5.3